THE JOURNAL OF PHYSICAL CHEMISTRY C

Article

pubs.acs.org/JPCC

Mechanism for Oxygen Reduction Reaction on Pt_3Ni Alloy Fuel Cell Cathode

Yao Sha,[†] Ted H. Yu,[†] Boris V. Merinov,*[,†] Pezhman Shirvanian,[‡] and William A. Goddard, III*[,†]

[†]Materials and Process Simulation Center, MC 139-74, California Institute of Technology, Pasadena, California 91125, United States

[‡]Ford Motor Co., Research & Advanced Engineering, 2101 Village Road, Dearborn, Michigan 48104, United States

ABSTRACT: We use quantum mechanics, density functional theory at the PBE level, to predict the binding-site preferences and reaction barriers for all intermediates involved in the oxygen reduction reaction (ORR) on the low energy surface of Pt_3Ni alloy. Here we calculate that the surface layer is Ni depleted (100% Pt) while the second layer is Ni enriched (50% Pt) as shown by experiment. Even though the top layer is pure Pt, we find that the sublayer Ni imposes strong preferences in binding sites for most intermediates, which in turn strongly influences the reaction barriers. This strong preference leads to a strong site dependence of the barriers. Considering water as the solvent, we predict that, at low coverage of O_{ad} and OH_{ad}, the barrier for the rate-determining step is 0.81 eV, whereas, at high coverage, this barrier decreases to 0.43 eV. It can be compared to a barrier of 0.50 eV for pure Pt, explaining the improved ORR rate for the Pt_3Ni alloy. We report the results both for gas phase and for aqueous phase environments.

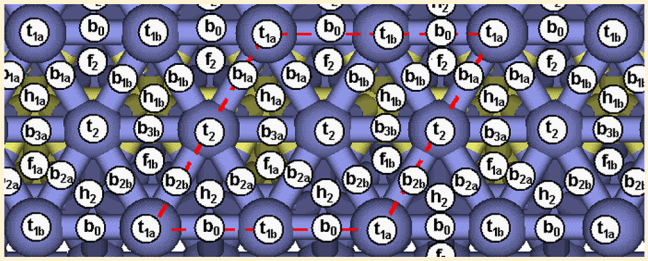

1. INTRODUCTION

The efficiency of the oxygen reduction reaction (ORR), $4H^+ + 4e^- + O_2 \rightarrow 2H_2O$, at the cathode of a polymer electrolyte membrane fuel cell (PEMFC) is a critical issue for commercial application of this type of fuel cells.[1−4] The best current catalysts are Pt and Pt-based binary alloys, such as Pt_3Ni.[5,6] The origin of the superior performance of the Pt_3Ni alloy has not been clearly understood yet. Some researchers believe it is due to the shift of the d-band center to the desired region that occurs due to alloying Pt with Ni.[7,8] Others came to the conclusion that alloying makes OH_{ad} removal favorable, increasing the surface area available for O_2 binding.[5] It has also been argued that alloying Pt with Ni or Co decreases the surface lattice parameters to values optimal for ORR.[9] A prominent property of Pt_3Ni and Pt_3Co is the strong surface segregation observed in experiments.[10−12] Our quantum mechanics (QM) calculations, density functional theory (DFT) at the Perdew−Becke−Ernzerhof (PBE) level, using a two-dimensional slab model find the similar segregation effect for the Pt_3Ni alloy which results in the surface structure with 100% Pt in the first layer, 50% Pt in the second layer, and 75% Pt in deeper layers.[13] This strong segregation to form a pure Pt surface layer (similar to core−shell systems where the surface is also pure Pt) is supposed to be important in ensuring the improved ORR activity of these alloy catalysts. A recent study of Matanovic et al.[14] argues that the sublayer concentration directly influences the overpotential. However, to our knowledge, no papers have been published that explore the influence of the atomic level configuration for alloying atoms to the reaction mechanism and barriers simultaneously by taking into account solvent effects.

In our study, we used QM calculations to study the unique binding-site preferences due to the placement of sublayer alloying atoms for all intermediates involved in the ORR on the segregated surface of Pt_3Ni and the consequent changes to the reaction barriers and mechanisms. We propose a new detailed atomistic level chemical mechanism explaining the increased reactivity of the Pt_3Ni alloy. In particular, we show that subsurface Ni has a strong influence on the binding energies and induces a coverage dependence for the preferred ORR mechanism.

2. METHODOLOGY

The $Pt_3Ni(111)$ alloy surface was modeled as a two-dimensionally infinite periodic slab with four atoms per cell and six layers of atoms. We consider the atomic Pt composition as 100-50-75-75-75-75% Pt, as observed experimentally[10] and calculated theoretically.[13,15,16]

All calculations used the PBE functional of DFT. We applied small core norm-conserving angular momentum projected pseudopotentials[17−20] in which the 3p, 3d, and 4s electrons of Ni and the 5p, 5d, and 6s electrons on the Pt are treated explicitly with 16 electrons for neutral Ni and Pt. The SeqQuest software[21] with optimized double-ζ plus polarization quality Gaussian-type orbitals on Pt and Ni was employed for our calculations. The periodic cell parameter of the slab corresponds to that of the optimized Pt_3Ni bulk structure and 0.08% smaller than the experimental value.[22] All charges came from the Mulliken population analysis of the DFT wave function.

Received: April 24, 2012
Revised: August 30, 2012
Published: September 4, 2012

dx.doi.org/10.1021/jp303966u | J. Phys. Chem. C 2012, 116, 21334−21342

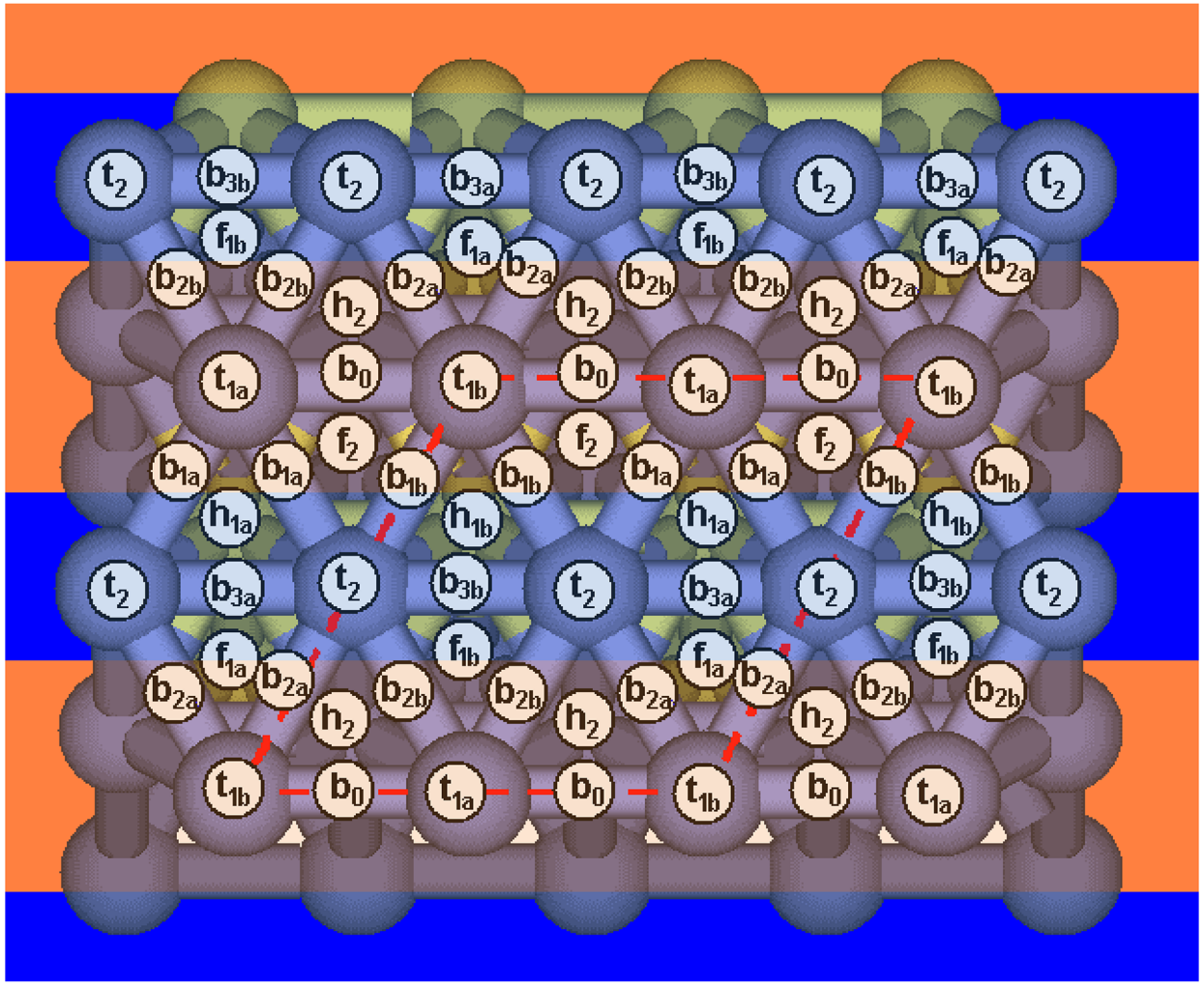

Figure 1. Binding sites on the $Pt_3Ni(111)$ surface. The blue and orange stripes indicate the partitioning of the Pt surface into two regions induced by the sublayer Ni. The O_2, O, H, OH, and OOH species prefer to move only within the orange stripes.

To represent the effects of solvent stabilization, we use the implicit model developed earlier.[23] The Mulliken charges were used as inputs to our implicit continuum solvation model based on the Poisson−Boltzmann equation. We showed that this implicit solvation model[23] correctly reproduces the solvation energies of O_{ad}, H_{ad}, OH_{ad}, and H_2O_{ad} calculated using explicit water layers. Implicit solvation can be applied both with periodic boundary conditions and for finite systems. Using explicit water requires thousands of water molecules to be treated dynamically, which is not yet practical with current QM methods. Solvation greatly affects the kinetics of the ORR on Pt and Pd surfaces. Theoretically, without solvation, Pd would outperform Pt as the ORR catalyst.[23] We use the same approach in this study and expect that charge transfer between Pt and Ni atoms may induce even larger dipoles and hence more significant solvent effects.

The barriers were calculated applying the nudged elastic band (NEB) method.[24,25] The energy, required to move a surface species (from a remote unit cell) to the starting site, is considered in deciding the preferred mechanism so that the site energy would not dominate the barrier. However, this site energy is not included in the barrier, because otherwise the barriers would correspond to the barriers for extremely low coverage. The reactants are assumed to be inside the same unit cell.

3. RESULTS AND DISCUSSION

3.1. Binding of ORR Intermediates. *3.1.1. Binding Site Notation.* First, we studied the preference of H, O, OH, H_2O, O_2, and OOH on various binding sites shown in Figure 1. Generally, a closest packed (111) surface of FCC structured metals has four types of sites:

- on-top, bonded to one Pt (μ_1), denoted as t
- bridging, between two Pt (μ_2), denoted as b
- bridging, between three Pt (μ_3) but in the FCC position (not above atoms of the top or second layer), denoted as f
- bridging, between three Pt (μ_3) but in the HCP position (above atoms of the second layer), denoted as h

However, due to strong segregation, the Pt_3Ni surface has 100% Pt in the first layer, 50% Ni and 50% Pt in the second layer, and 25% Ni and 75% Pt in the four remaining layers. We find that the binding energies of the intermediates to the pure Pt layer strongly depend on the nature of the second layer atoms. The various cases are tabulated in Figure 1. Figure 2 shows details of the difference between sites.

For the first and second layers, there are two types of top sites: t_1 with one Ni neighbor in the second layer and t_2 with two Ni neighbors. Considering also the third layer, we can distinguish t_{1a} with no Ni in the third layer directly beneath

dx.doi.org/10.1021/jp303966u | J. Phys. Chem. C 2012, 116, 21334−21342

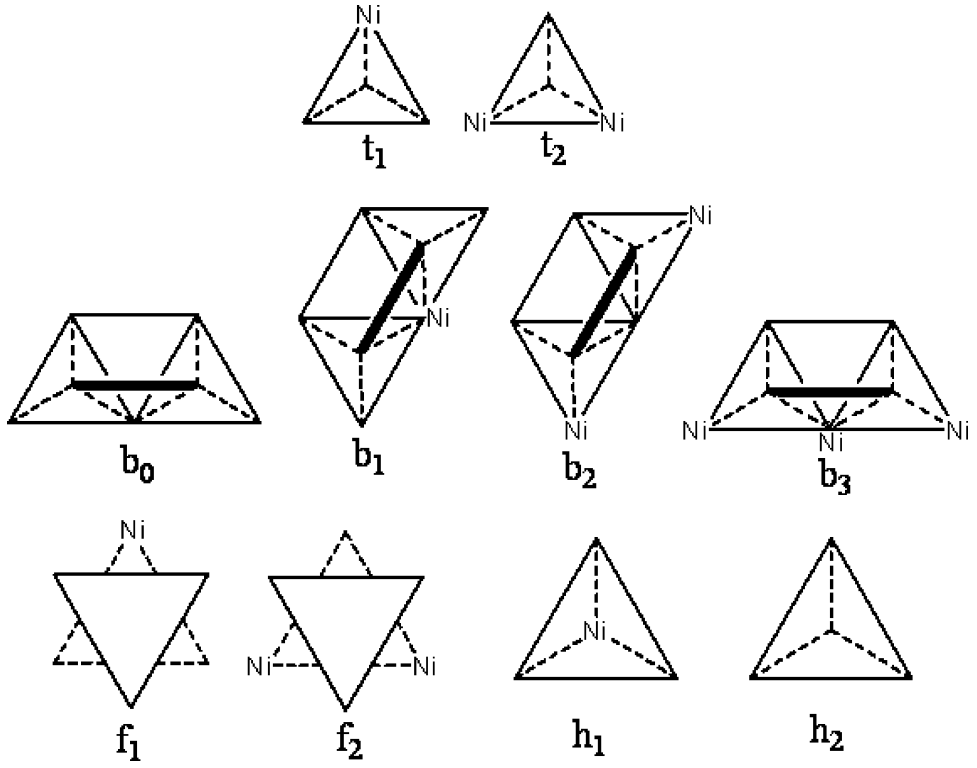

Figure 2. Illustration of various binding sites on the $Pt_3Ni(111)$ surface. For top sites t_1 and t_2, the triangle indicates the sublayer atoms. t_1 has one Ni atom beneath it, while t_2 has two. For bridge sites, the bridge itself is shown as the thick black line, while the two termini of the black line connect the two surface atoms forming the bridge site. The trapezoids beneath are sublayer atoms. b_0–b_3 have from 0 to 3 Ni atoms in the sublayer. An FCC site is in the center of a surface triangle (shown as a solid triangle). f_1 and f_2 differ in the sublayer triangle beneath the surface triangle. f_1 has one Ni beneath it, while f_2 has two. HCP sites are also in the center of a surface triangle. They have one sublayer atom beneath it. For h_1, it is Ni, while, for h_2, it is Pt.

the surface and t_{1b} with one Ni. All t_2 sites are the same (see Figure 2).

For the top two layers, there are four μ_2 bridge sites, depending on the number of Ni atoms underneath it: b_0, b_1, b_2, and b_3 with 0, 1, 2, and 3 Ni atoms in the second layer. With adding the third layer, there appear to be two subtypes for b_1, b_2, and b_3, depending on the distance to the Ni atom in the third layer. We denote the subtypes closer to the third layer Ni as b_{1a}, b_{2a}, and b_{3a} and the others as b_{1b}, b_{2b}, and b_{3b}, respectively (Figure 2).

Considering only two top layers, two FCC sites can be distinguished: f_1 and f_2 with one and two Ni atoms in the sublayer triangle, but adding the third layer splits f_1 into f_{1a} and f_{1b} with f_{1a} on top of the third layer Ni and f_{1b} on top of the third layer Pt.

Similarly, there are two HCP sites related to the two top layers: h_1 and h_2. Here, h_1 is on top of the Ni sublayer, while h_2 is on top of the Pt sublayer. Adding the third layer splits the h_1 site into h_{1a} and h_{1b} with one Ni atom and without Ni atoms in the projected triangle of the third layer atoms, as shown in Figure 2.

All the above sites can be partitioned into two categories: the sites closer to the sublayer Pt atoms (the orange region in Figure 1) and the sites closer to the sublayer Ni atoms (the blue region in Figure 1). As we will show later, the orange region is universally preferred.

The binding energies (BE) are calculated as the energy gain for species to adsorb to the surface, i.e.,

$$BE_{gas} = E_{surf+M,gas} - E_{surf,gas} - E_{M,gas}$$

where M is an adsorbate. For the solution phase, the solvent stabilization is added directly to the binding energy in order to isolate the influence of water. This leads to

$$BE_{solv} = E_{surf+M,solv} - E_{surf,solv} - E_{M,gas}$$

The solvent phase binding energy does not include the solvent effect of the adsorbate itself, because most of the species are radicals that do not have well-defined solvation energies for comparison. The lack of these energy data for radical species does not affect the barrier calculations, since the reactants, products, and transition states are all surface species and the differences in individual solvation energies eventually cancel out.

All barriers are calculated as the energy difference between a transition state and surface reactants. We disregard the energy that reactants need to migrate from the globally preferred sites to the reacting sites, as this barrier would correspond only to very low coverage. This condition is not typical for conventional fuel cell operation.

3.1.2. H Binding. The preferred binding site for H on the Pt_3Ni surface is t_{1a} with a binding energy of 2.70 eV, followed by t_{1b} and b_0 with a binding energy of 2.60 eV in the gas phase.

On the other hand, the b_{3a}, b_{3b}, and t_2 sites in the orange region have binding energies of 2.39–2.44 eV in the gas phase, 0.26–0.31 eV weaker than the binding energy of the preferred binding site. The barrier for H_{ad} migration within the orange region ($b_0 \rightarrow t_{1a} \rightarrow b_0 \rightarrow t_{1b} \rightarrow b_0$) is approximately 0.10 eV, while the barrier for H_{ad} to migrate between adjacent orange regions (through the blue region) is 0.26 eV. Hence, hydrogen prefers to stay within the orange region. We will show below

dx.doi.org/10.1021/jp303966u | J. Phys. Chem. C 2012, 116, 21334–21342

that this preference is universal for all surface species. For clarity, the orange region is denoted as "the preferred region".

Under solvation, the preferred sites become t_{1a}, b_{1a}, and f_{1b}, with binding energies of 2.78−2.83 eV, followed by t_{1b}, b_0, b_{1ab}, f_2, h_{1a}, h_{1ab}, and h_2 with binding energies of 2.68−2.74 eV.

The b_{3a}, b_{3b}, and t_2 sites in the orange region have a binding energy of 2.48−2.54 eV under solvation, which is weaker by 0.3 eV than that of the preferred binding site.

Comparing with the gas phase results, we conclude that solvation does not alternate the preferred region (orange region). The barrier for the H_{ad} migration within the orange region is as low as 0.08 eV, while the barrier for H_{ad} to migrate between adjacent orange regions is 0.30 eV. The difference of 0.22 eV is higher than the corresponding difference of 0.16 eV for the gas phase. Therefore, solvation makes migration between adjacent orange regions more difficult. Consequently, the blue region serves as a barrier region preventing hydrogen from diffusing between different orange stripes.

For the pure Pt surface, the binding energy of H is 2.70−2.80 eV in the gas phase and 2.81−2.81 eV in the solvated phase. There are no "forbidden" regions in this case. This allows H_{ad} to migrate easily in all directions to react with other species.

3.1.3. O Binding. On pure Pt, O_{ad} binds strongly to the FCC site with a net energy of 3.66 eV in the gas phase and 4.36 eV in the solvated phase. The huge solvation stabilization arises from electrostatics due to appearance of the strong dipole at surface O_{ad} atoms.

For Pt_3Ni, the binding energy for O_{ad} depends dramatically on the site. The f_2 site is preferable in the gas phase with a binding energy of 3.47 eV, followed by the f_{1a} site with a binding energy of 3.17 eV. The next best sites in the gas phase are b_0, f_{1b}, and h_2, which are weaker than f_2 by 0.40 eV.

With solvent, f_2 and f_{1b} become dominant with binding energies of 4.49 and 4.28 eV, respectively. All other binding sites are at least 0.60 eV less stable than f_2 and have small barriers for O to migrate into the f_2 site, except for the case with extremely high coverage. The strong stabilization of the f_2 site is due to two electropositive Ni with the Mulliken charge of 0.14−0.18e in the second layer that enhance the charge transfer to the surface O_{ad}, stabilizing it. This is illustrated by the surface total charge of 0.079 on f_1 and 0.114 on f_{2a} and f_{2b}.

The binding energy for the FCC site on the pure Pt surface is 0.19 eV stronger than that for the f_2 site in the gas phase but 0.13 eV weaker with solvation.

The smaller Ni atoms allow the surface Pt above two Ni to contract the distance by 0.29 Å toward the bulk values, whereas the corresponding change for the surface Pt above one Ni is 0.19 Å.

These results indicate that O_{ad}, formed from O_2 dissociation, strongly prefers to occupy the f_2 site and no further migration occurs to the other sites both in the gas phase and solution.

3.1.4. OH Binding. On pure Pt, OH has almost the same binding energy at all sites, 2.22−2.28 eV in the gas phase and 2.57−2.77 eV in solution.

For Pt_3Ni, the best site in the gas phase is b_0 with a binding energy of 2.42 eV. Here, the OH-bond tilts toward h_{1b} (away from f_2). The t_{1a}, t_{1b}, f_2, h_2, and b_{1a} sites are less stable than b_0 by 0.10−0.20 eV. The barrier for OH to migrate across the preferred regions is 0.29 eV, while the barrier for OH migration within the same preferred region is negligible. Hence, similar to the H binding, OH selectively binds and stays within the preferred region.

With solvation, t_{1a} is the most preferred site with a binding energy of 2.83 eV, followed by f_2, b_0, and t_{1b} with a binding energy of 2.73−2.75 eV. For comparison, OH binds much weaker to t_2, b_{3a}, and b_{3b} with a binding energy of 2.24−2.47 eV. Thus, the preferred region remains the same as in the gas phase (orange region in Figure 1). The in-region OH_{ad} migration barrier is 0.10 eV, and the across-region barrier is 0.36 eV (estimated by the binding energy of b_{3a} and b_{3b}).

At the other binding sites, OH_{ad} has a strong preference to migrate to the preferred region. This differs dramatically from the case of the pure Pt surface where the binding energy of OH at all possible sites ranges within 0.06 eV in the gas phase and 0.20 eV in the solvated phase, indicating the ability for easy OH migration.

3.1.5. O_2 Binding. For pure Pt, we find that the binding energy of O_2 is 0.46 eV in the gas phase and 0.87 eV in the solvated phase, with the difference for various sites ranging within 0.11 and 0.17 eV for gas phase and solution, respectively.

For the Pt_3Ni surface, O_2 binds most strongly to b_0, b_{1a}, b_{1b}, and f_2 in the gas phase. The corresponding binding mmaenergies vary from 0.33 to 0.59 eV in the gas phase and from 0.62 to 0.76 eV in solution. All other sites are less favorable by at least 0.3 eV. Thus, O_2 has a small preferred binding region near the f_2 site on Pt_3Ni which is adjacent to the f_2 site for O_{ad} and to the b_0 site for OH_{ad}. This small region is part of the preferred region (orange region), and the barrier to migrate between preferred regions is at least 0.32 eV in the gas phase and 0.38 eV in the solvated phase (estimated by the binding energy of b_{3a} and b_{3b}).

Given that H also prefers this region and would likely be nearby, this implies a favorable migration pathway for OOH formation.

3.1.6. OOH Binding. For pure Pt, OOH binds to the top sites with the terminal O bonded to the Pt and the OOH plane parallel to the surface. OOH prefers to have the O−O bond heading to an adjacent Pt atom. This leads to a binding energy of 1.06 eV in the gas phase and 1.52 eV in solution.

For Pt_3Ni, we find that t_{1a} is quite favorable with the binding energy of 1.05 eV in the gas phase and 1.55 eV in the solvated phase. Here the preferred orientation for the O−O bond is also toward the adjacent Pt atom, similar to pure Pt.

All other sites are not reachable for OOH, leading instead to dissociation. Thus, once formed, OOH cannot migrate on the surface.

3.1.7. H_2O Binding. H_2O binds only to top sites with binding energies of 0.18−0.20 eV in the gas phase and 0.57−0.60 eV in solution, all close to the corresponding values of 0.22 and 0.58 eV for pure Pt. Comparing with the 0.40 eV solvent stabilization of bulk H_2O, the surface H_2O shows positive binding in both cases.

Since H_2O does not bind to bridge, FCC, and HCP sites, migration of H_2O_{ad} from one top site to another is through adsorption and dissociation. The migration barrier is 0.20 eV both in the gas phase and solution (the 0.60 eV binding energy minus the 0.40 eV solvation of H_2O_{ad}, H_2O is considered always solvated).

3.1.8. H_2O_2 Binding. H_2O_2 has a binding energy of 0.23−0.31 eV on the Pt_3Ni surface in the gas phase and 0.58−0.67 eV in the solvated phase, close to the 0.27 and 0.61 eV for pure Pt. Similar to the H_2O case, H_2O_2 migrates through desorption and readsorption.

3.1.9. Summary of Binding. Summarizing, we find (see Tables 1 and 2) that

- O strongly prefers f_2.
- O_2 can occupy the b_0, b_{1a}, b_{1b}, and f_2 sites.
- H prefers to move within in the orange region, allowing it to attack O at the f_2 site to form OH at the b_0, t_{1a}, or t_{1b} sites.

dx.doi.org/10.1021/jp303966u | J. Phys. Chem. C 2012, 116, 21334−21342

Table 1. Binding Energies (eV) of ORR Intermediates at Different Sites on Pt_3Ni and Pt in the Gas Phase

BE	BE	H	O	OH	O_2	OOH	H_2O	H_2O_2
Pt_3Ni	t_{1a}	−2.70	−2.48	−2.29		−1.05[a]	−0.20	
	t_{1b}	−2.60	−2.37	−2.22		−0.97[a]	−0.18	
	t_2	−2.44	−2.16	−2.00		−0.98[a]	−0.18	
	b_0	−2.60	−3.09	−2.42	−0.59			−0.23
	b_{1a}	−2.57	−2.98	−2.25	−0.47			−0.29
	b_{1b}	−2.48	−2.95	−2.10	−0.39			−0.29
	b_{3a}	−2.39	−2.67	−1.96	−0.26			−0.29
	b_{3b}	−2.39	−2.62	−1.85	−0.24			−0.29
	b_{2a}	−2.46	−2.76	−1.98	−0.27			−0.31
	b_{2b}	−2.52	−2.75	−2.01	−0.25			−0.31
	f_2	−2.55	−3.47	−2.29	−0.33			
	f_{1a}	−2.45	−3.17	−1.92	0.04			
	f_{1b}	−2.49	−3.08	−1.89	0.00			
	h_{1a}	−2.48	−2.96	−1.90	−0.18			
	h_{1b}	−2.47	−2.94	−1.87	−0.09			
	h_2	−2.53	−3.06	−2.32	−0.15			
	best	−2.70	−3.47	−2.42	−0.59	−1.05	−0.20	−0.31
Pt	t	−2.80	−2.50	−2.23		−1.06	−0.22	
	b	−2.70	−3.10	−2.25	−0.40			−0.27
	f	−2.72	−3.66	−2.22	−0.46			
	h	−2.70	−3.28	−2.28	−0.35			
	best	−2.80	−3.66	−2.28	−0.46	−1.06	−0.22	−0.27

[a]OOH can have two orientations: the O−O bond points toward an adjacent Pt atom (preferred, binding energy shown) or toward an FCC/HCP site (binding energies 0.93, 0.77, and 0.78 eV, respectively).

Table 2. Binding Energies (eV) of ORR Intermediates at Different Sites on Pt_3Ni and Pt in Solution

BE	sites	H	O	OH	O_2	OOH	H_2O	H_2O_2
Pt_3Ni	t_{1a}	−2.78	−3.10	−2.83		−1.55[a]	−0.61	
	t_{1b}	−2.70	−2.95	−2.73		−1.46[a]	−0.57	
	t_2	−2.48	−2.66	−2.47		−1.45[a]	−0.58	
	b_0	−2.70	−3.70	−2.74	−0.75			−0.58
	b_{1a}	−2.83	−3.82	−2.64	−0.66			−0.63
	b_{1b}	−2.69	−3.79	−2.55	−0.62			−0.64
	b_{3a}	−2.48	−3.25	−2.30	−0.36			−0.64
	b_{3b}	−2.54	−3.50	−2.24	−0.37			−0.63
	b_{2a}	−2.57	−3.35	−2.32	−0.39			−0.66
	b_{2b}	−2.63	−3.38	−2.33	−0.40			−0.67
	f_2	−2.74	−4.49	−2.75	−0.76			
	f_{1a}	−2.55	−3.80	−2.27	−0.20			
	f_{1b}	−2.77	−4.28	−2.28	−0.34			
	h_{1a}	−2.69	−3.69	−2.25	−0.38			
	h_{1b}	−2.74	−3.89	−2.31	−0.30			
	h_2	−2.68	−3.66	−2.66	−0.38			
	best	−2.83	−4.49	−2.83	−0.76	−1.55	−0.61	−0.67
Pt	t	−2.87	−3.09	−2.77		−1.52	−0.58	
	b	−2.82	−3.73	−2.63	−0.73			−0.61
	f	−2.85	−4.36	−2.57	−0.87			
	h	−2.81	−3.92	−2.64	−0.70			
	best	−2.87	−4.36	−2.77	−0.87	−1.52	−0.58	−0.61

[a]Same notes as for Table 1 except that the binding energies are 1.42, 1.24, and 1.32 eV.

- OH can also move through b_0, t_{1a}, t_{1b}, f_2, and h_2.
- OOH occupies top sites with the second O orienting nearby Pt.
- H_2O prefers all top sites, while H_2O_2 does bridge sites.

These imply a strong regional preference for O_2, O, H, OH, and OOH to stay in the orange stripes. Of the top sites, t_{1a} and t_{1b} are most preferable for all species. Similarly, b_0 is predominantly preferred among bridge sites. Among the 3-fold FCC, HCP, f_{1a}, f_{1b}, f_2, h_{1a}, h_{1b}, and h_2 binding sites, f_2 is most favorable. Thus, at lower coverage (quarter layer), the b_0, f_2, and t_{1a} (also t_{1b}) sites are preferred, when the surface is exposed to all the intermediates. Only at higher coverage, the adsorbates bind to other sites.

Therefore, the chemistry prefers the orange region. The direct consequence of this is that reaction barriers depend on whether the starting and ending sites are inside or outside of the preferred region. This conclusion also agrees with the experimental result

obtained by Markovic et al.[5] on $Pt_3Ni(111)$, where the fractional coverages of the underpotentially deposited hydrogen and adsorbed hydroxyl species were dramatically decreased by 50% as compared to Pt(111). The blue region has much lower binding energy and hence is much lower covered with H_{ad} and OH_{ad}.

3.2. Reaction Barriers and Possible ORR Mechanisms. Our previous studies[13,23,26,27] showed that six fundamental steps can be involved in the ORR mechanism:

(a) O_2 dissociation: $O_{2ad} \rightarrow O_{ad} + O_{ad}$
(b) OH formation: $O_{ad} + H_{ad} \rightarrow OH_{ad}$
(c) H_2O formation: $OH_{ad} + H_{ad} \rightarrow H_2O_{ad}$
(d) OOH formation: $O_{2ad} + H_{ad} \rightarrow HOO_{ad}$
(e) OOH dissociation: $HOO_{ad} \rightarrow OH_{ad} + O_{ad}$
(f) Hydration: $O_{ad} + H_2O_{ad} \rightarrow OH_{ad} + O_{ad}$

By including these fundamental steps in an overall mechanism, we distinguish three chemical processes:

O−O bond activation, which can occur via two mechanisms: (1) O_2 dissociation (a) and (2) OOH formation (d) followed by OOH dissociation (e).

OH formation proceeds via two mechanisms as well: OH formation (b) and O hydration (f).

OH consumption. There is only one mechanism, H_2O formation (c), for this process.

A good catalyst must provide low barriers for all three of these processes and for pathways connecting them.

Starting from the preferred sites, we calculated the barriers for all six steps on Pt_3Ni in the gas phase and solution. These barriers and their comparison with those for pure Pt are shown in Tables 3 and 4.

Table 3. Reaction Barriers (eV) for ORR Steps on Pt_3Ni and Pt Surfaces in the Gas Phase

reaction barriers	Pt	Pt_3Ni	high coverage
H_2 dissociation	0.00	0.05	
O_2 dissociation	0.58	1.02	0.92
OH formation	0.72	0.57	0.67
H_2O formation	0.11	0.11	0.36
OOH formation	0.28	0.32	
OOH dissociation	0.14	0.04	
H−OOH dissociation	0.18	0.20	
O hydration[a]	0.29	0.34	0.00

[a]The O hydration on Pt is calculated using a 3 × 3 cell, because a 2 × 2 cell is not large enough. For Pt_3Ni, we used 4 × 2 and 2 × 4 cells to keep the correct periodic condition.

Table 4. Reaction Barriers (eV) for ORR Steps on Pt_3Ni and Pt Surfaces in Solution

reaction barriers	Pt	Pt_3Ni	high coverage
H_2 dissociation	0.00	0.01	
O_2 dissociation	0.00	0.00	0.24
OH formation	1.09	1.02	0.80
H_2O formation	0.17	0.25	0.43
OOH formation	0.19	0.17	
OOH dissociation	0.00	0.00	
H−OOH dissociation	0.04	0.22	
O hydration[a]	0.50	0.81	0.44

[a]Same notes as for Table 3.

3.2.1. Gas Phase Barriers for Pt_3Ni at Low Coverage. O−O Bond Activation. OOH formation with a barrier of 0.32 eV is followed by OOH dissociation with a very small barrier of 0.04 eV, whereas the barrier for the direct dissociation is 1.02 eV. This is similar to the case of pure Pt where OOH formation has a barrier of 0.28 eV compared to 0.58 eV for direct dissociation.

OH Formation. O hydration has a barrier of 0.34 eV, compared to 0.57 eV for the direct OH formation. This preference for the O hydration is similar to the case of pure Pt where the O hydration barrier is 0.29 eV compared to 0.72 eV for the direct OH formation.

OH Consumption. H_2O formation has a small barrier of 0.11 eV, exactly the same as for the pure Pt case.

Summarizing these three steps, we have the following preferred mechanism (denoted as OOH-form-hydr-gas) for both Pt_3Ni and Pt.

$$O_{2ad} + H_{ad} \rightarrow OOH_{ad}$$
(E_a = 0.32 eV for Pt_3Ni and 0.28 eV for Pt)

$$OOH_{ad} \rightarrow O_{ad} + OH_{ad}$$
(E_a = 0.04 eV for Pt_3Ni and 0.14 eV for Pt)

$$O_{ad} + H_2O_{ad} \rightarrow 2OH_{ad}$$
(E_a = 0.34 eV for Pt_3Ni and 0.29 eV for Pt)

$$OH_{ad} + H_{ad} \rightarrow H_2O_{ad}$$
(E_a = 0.11 eV for Pt_3Ni and 0.11 eV for Pt)

Figure 3 shows the potential energy surface of this preferred mechanism both on Pt and Pt_3Ni surfaces. The rate-determining step (RDS) for this mechanism is the O hydration with a barrier of 0.34 eV for Pt_3Ni and 0.29 eV for pure Pt. Hence, for the gas phase, Pt outperforms Pt_3Ni.

3.2.2. Gas Phase Barriers for Pt_3Ni at Higher Coverage. At higher coverage in the gas phase, the situation does not change significantly compared to the low coverage. The ORR mechanism remains the same except for the RDS which is now the water formation with a barrier of 0.36 eV, while at the low coverage it is the O hydration step with a slightly lower barrier of 0.34 eV (see Table 3).

3.2.3. Solvated Phase Barriers for Pt_3Ni at Low Coverage. O−O Bond Activation. The best O_2 dissociation pathway starts from an f_2-bound O_2 which dissociates to form two O_{ad} at f_2 sites with no barrier (because solvent strongly favors dissociation), similar to that on pure Pt. We find that OOH formation has a barrier of 0.17 eV on Pt_3Ni, close to 0.19 eV on pure Pt. OOH dissociation is barrierless on Pt_3Ni, similar to that on Pt. Thus, the OOH formation and dissociation are not unfavorable pathways for the solvated system.

OH Formation. For the second step, Pt_3Ni has a direct OH formation barrier of 1.02 eV, slightly lower than 1.09 eV on pure Pt. The O hydration step is less favorable on Pt_3Ni, leading to a barrier of 0.81 eV, compared to 0.50 eV for pure Pt. Earlier,[22] we showed that the O hydration is the dominant mechanism for forming OH on Pt. Hence, the O hydration is the preferred mechanism for both Pt_3Ni and Pt with a barrier of 0.81 and 0.50 eV, respectively. This suggests that Pt_3Ni would have a worse performance for formation of OH_{ad}.

OH Consumption. For the consumption of OH, water formation on Pt_3Ni with a barrier of 0.25 eV is slightly worse than that on Pt (the barrier is 0.17 eV).

dx.doi.org/10.1021/jp303966u | J. Phys. Chem. C 2012, 116, 21334−21342

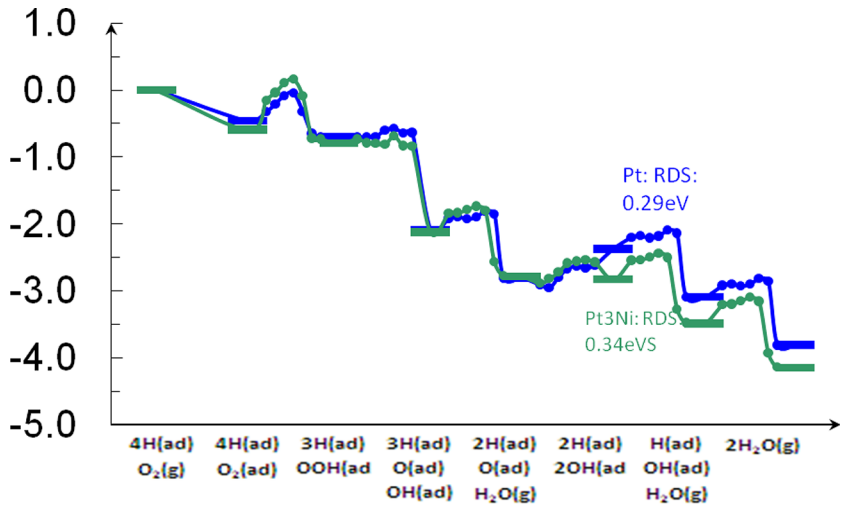

Figure 3. Potential energy surface including barriers for the OOH-form-hydr mechanism preferred for both Pt and Pt_3Ni in the gas phase.

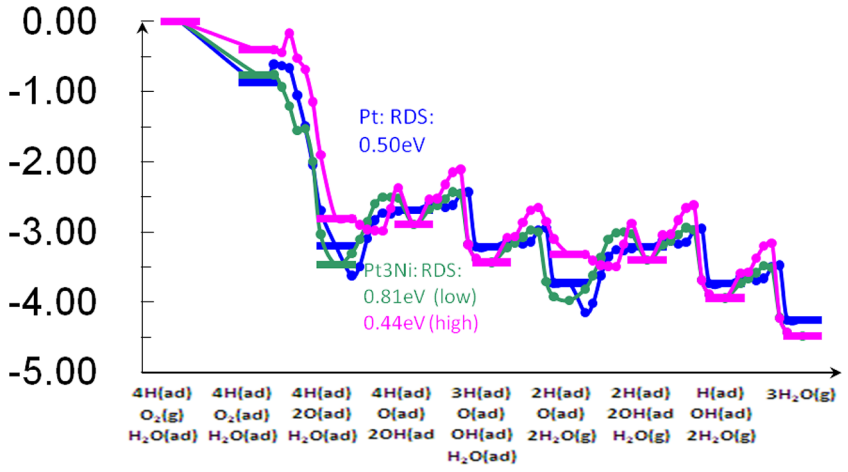

Figure 4. Potential energy surface including barriers for the O_2-diss-hydr mechanism preferred for both Pt_3Ni and Pt in solution. The purple line shows the alternative mechanism at higher coverage.

Summarizing the above discussion, we come to the conclusion that the O_2-diss-hydr-low mechanism is favorable in the solvated phase:

$$O_{2ad} \rightarrow 2O_{ad} \quad (E_a = 0.00 \text{ eV both for } Pt_3Ni \text{ and Pt})$$

$$O_{ad} + H_2O_{ad} \rightarrow 2OH_{ad} \quad (E_a = 0.81 \text{ eV for } Pt_3Ni \text{ and } 0.50 \text{ eV for Pt})$$

$$OH_{ad} + H_{ad} \rightarrow H_2O_{ad} \quad (E_a = 0.25 \text{ eV for } Pt_3Ni \text{ and } 0.17 \text{ eV for Pt})$$

Figure 4 shows the potential energy surface of the O_2-diss-hydr-low mechanism with solvent effects at different coverage. In solution, the O hydration is the RDS for both Pt_3Ni and Pt with the overall barrier of 0.81 and 0.50 eV, respectively. Thus, our computation suggests that Pt_3Ni would not outperform Pt. This result disagrees with the experimental observation, showing that Pt_3Ni is a more efficient ORR catalyst than pure Pt.[5]

3.2.4. Solvated Phase Barriers for Pt_3Ni at Higher Coverage. The above analysis is based on the assumption that all reactants are at the preferred sites, i.e., the reactants are within the orange region in Figure 1. In contrast, at higher coverage, the reactants might end up in the blue region, even though it is not preferred at low coverage. The adsorbate coverage on the catalyst surface can range from 1/4 to as high as 2/3 monolayer.[28−30] At higher coverage, the blue region becomes accessible for binding. Actually, it is not necessary for the coverage to be higher than 1/4 monolayer to trigger binding to the less preferred sites, because the large migration barrier may also block the rearrangement of O atoms toward adjacent sites (the O migration barrier between f_2 sites is 0.6 eV). To consider the changes that might occur at higher coverage, we calculated the corresponding barriers for the blue region.

For the O_2 dissociation starting from h_{1b}, O_2 can easily dissociate to form O_{ad} in the f_{1a} and f_{1b} sites with a barrier of 0.24 eV in solution and 0.92 eV in the gas phase.

For O_{ad} at the f_{1a} and f_{1b} sites, the corresponding O hydration reaction with nearby H_2O has a barrier of 0.44 eV in solution but is barrierless in the gas phase.

The following step of the H_2O formation also has a low barrier of 0.43 eV in the solvated phase and 0.36 eV in the gas phase.

Hence, when the preferred region is covered with O_{ad}, O_2 can start to bind to the unfavorable h_{1b} site, and then dissociate to f_{1a} and f_{1b}. This allows a lower barrier for the hydration step, $O_{ad} + H_2O_{ad} \rightarrow 2OH_{ad}$, avoiding the high O hydration

dx.doi.org/10.1021/jp303966u | J. Phys. Chem. C 2012, 116, 21334−21342

and OH formation barriers calculated for low coverage, 0.81 and 1.02 eV, respectively. The proposed mechanism is O_2-diss-hydr-high:

$$O_{2ad} \rightarrow 2O_{ad}$$
(E_a = 0.00 eV at low coverage and 0.24 eV at high coverage)

$$O_{ad} + H_2O_{ad} \rightarrow 2OH_{ad}$$
(E_a = 0.81 eV at low coverage and 0.44 eV at high coverage)

$$OH_{ad} + H_{ad} \rightarrow H_2O_{ad}$$
(E_a = 0.25 eV at low coverage and 0.43 eV at high coverage)

Figure 4 shows the potential energy surface of the O_2-diss-hydr mechanism in solution at different coverages. The overall mechanism has the O hydration as the RDS with a barrier of 0.44 eV, slightly smaller than 0.50 eV for pure Pt. This mechanism occurs on the $Pt_3Ni(111)$ surface at higher coverage.

Thus, in the gas phase, the preferred mechanism is OOH-form-hydr with a RDS barrier of 0.34 eV for Pt_3Ni and 0.29 eV for Pt. In solution at low coverage, where all intermediates can bind to the preferred region, we predict that Pt_3Ni would have slower kinetics than Pt with an overall barrier of 0.81 eV. However, at higher coverage, the less preferred (blue) region might be involved in the process, which leads to a RDS barrier of 0.44 eV, smaller than that of 0.50 eV for pure Pt. This result is consistent with experiment.

3.3. Origin of Improved Performance. Comparing the RDS barriers for Pt and Pt_3Ni, we can see that the major problem for both Pt and Pt_3Ni alloys as ORR catalyst is the slow OH formation step. At low coverage, the situation becomes even worse, because of the stronger binding of O_{ad} by 0.13 eV on Pt_3Ni as compared to pure Pt. This makes any step that converts O_{ad} into OH_{ad} more difficult on Pt_3Ni. However, at higher coverage or less organized coverage, when the favored sites are not all available, O atoms begin adsorbing onto the less favored blue region, which leads to a much lower reaction enthalpy and barrier for OH formation either via direct OH formation or O hydration. To reach better performance of Pt and Pt_3Ni catalysts, the OH formation barrier should be lowered. This agrees with the volcano-like trend for ORR catalysts,[7,31,32] when the activity first increases and then decreases as the catalyst d-band center shifts downward. A lower d-band center provides stronger binding of OH_{ad} and O_{ad}. A strong enough binding of O atom is required for O adsorption, but too strong binding makes OH formation (and probably H_2O formation) more difficult. Our study shows that Pt_3Ni has, on average, weaker O and OH binding, especially on the blue region. This is in agreement with earlier obtained results.[7,33]

From our calculation, we find more difficult water formation on Pt_3Ni compared to pure Pt, which is a much smaller issue when H^+ is involved in the reaction.[13,27,34] A weaker bonded OH would be easier removed by H^+. This is consistent with the assumption about a spatial effect;[5,35] easier OH removal leads to more surface area for O adsorption. However, our results show that the more difficult step for Pt_3Ni is O → OH, E_a = 0.80 and 0.44 eV via OH formation and O hydration, respectively, at high coverage (see Table 4) rather than the OH → H_2O step, E_a = 0.25−0.43 eV via direct formation and becomes negligible if H^+ is involved in the reaction.[34] These barriers are lower than the corresponding barriers for Pt (O_{ad} → OH_{ad}, E_a = 1.09 eV via direct OH formation and E_a = 0.50 eV via O hydration). The lower barriers lead to the improved performance.

4. CONCLUSIONS

We studied systematically the binding site preference of all reaction intermediates involved in ORR on Pt_3Ni. The binding energy of adsorbates on the alloy surface shows the strong sublayer dependence. Compared with the pure Pt surface, the binding sites are partitioned into two regions, the preferred (orange) and the less preferred (blue) region. The mechanism of ORR on Pt_3Ni is similar to that on pure Pt. In solvent, O_2 first dissociates into O_{ad}, then O_{ad} reacts with H_2O to produce OH_{ad}, which finally reacts with H_{ad} to form H_2O.

Due to the substantial difference in binding sites, ORR shows different kinetics for the preferred and less preferred regions. The overall barrier for ORR at the preferred region is 0.81 eV, while the barrier for the less preferred region is significantly lower, 0.43 eV. Thus, the ORR activity should be strongly coverage-dependent. At low coverage, all reactants and intermediates adsorb only onto the preferred region, generating a slower reaction rate than that on pure Pt. At higher coverage, O_2 can react at the less preferred region, leading to a better rate as compared to pure Pt.

AUTHOR INFORMATION

Corresponding Author

*E-mail: merinov@wag.caltech.edu (B.V.M.); wag@wag.caltech.edu (W.A.G.).

Notes

The authors declare no competing financial interest.

ACKNOWLEDGMENTS

This work was supported partially by the National Science Foundation under Grant CBET-1067848 (Program Manager: Dr. George Antos) and partially by Ford Motor Company. The facilities of the MSC used in this study were established with grants from DURIP-ONR, DURIP-ARO, and NSF-CSEM.

REFERENCES

(1) Kordesch, K.; Simader, G. *Fuel Cells and Their Applications*; VCH: New York, 1996.
(2) Appleby, A.; Foulkes, F. *Fuel Cell Handbook*; Van Nostrand Reinhold: New York, 1989.
(3) Brandon, N. P.; Skinner, S.; Steele, B. C. H. *Annu. Rev. Mater. Res.* **2003**, *33*, 183−213.
(4) Mehta, V.; Cooper, J. S. *J. Power Sources* **2003**, *114*, 32−53.
(5) Stamenkovic, V. R.; Fowler, B.; Mun, B. S.; Wang, G. F.; Ross, P. N.; Lucas, C. A.; Markovic, N. M. *Science* **2007**, *315*, 493−497.
(6) Stamenkovic, V.; Schmidt, T. J.; Ross, P. N.; Markovic, N. M. *J. Phys. Chem. B* **2002**, *106*, 11970−11979.
(7) Stamenkovic, V.; Mun, B. S.; Mayrhofer, K. J. J.; Ross, P. N.; Markovic, N. M.; Rossmeisl, J.; Greeley, J.; Norskov, J. K. *Angew. Chem., Int. Ed.* **2006**, *45*, 2897−2901.
(8) Greeley, J.; Norskov, J. K. *J. Phys. Chem. C* **2009**, *113*, 4932−4939.
(9) Yang, H.; Vogel, W.; Lamy, C.; Alonso-Vante, N. *J. Phys. Chem. B* **2004**, *108*, 11024−11034.
(10) Gauthier, Y.; Joly, Y.; Baudoing, R.; Rundgren, J. *Phys. Rev. B* **1985**, *31*, 6216−6218.
(11) Gauthier, Y. *Surf. Rev. Lett.* **1996**, *3*, 1663−1689.
(12) Bardi, U.; Atrei, A.; Zanazzi, E.; Rovida, G.; Ross, P. N. *Vacuum* **1990**, *41*, 437−440.

(13) Yu, T.; Sha, Y.; Merinov, B.; Goddard, W., III. *J. Phys. Chem. C* **2010**, *114*, 11527−11533.
(14) Matanovic, I.; Garzon, F. H.; Henson, N. J. *J. Phys. Chem. C* **2011**, *115*, 10640−10650.
(15) Ma, Y. G.; Balbuena, P. B. *J. Phys. Chem. C* **2008**, *112*, 14520−14528.
(16) Mun, B. S.; Watanabe, M.; Rossi, M.; Stamenkovic, V.; Markovic, N. M.; Ross, P. N. *Surf. Rev. Lett.* **2006**, *13*, 697−702.
(17) Melius, C. F.; Goddard, W. A. *Phys. Rev. A* **1974**, *10*, 1528−1540.
(18) Melius, C. F.; Olafson, B. D.; Goddard, W. A. *Chem. Phys. Lett.* **1974**, *28*, 457−462.
(19) Redondo, A.; Goddard, W. A.; Mcgill, T. C. *Phys. Rev. B* **1977**, *15*, 5038−5048.
(20) Hamann, D. R. *Phys. Rev. B* **1989**, *40*, 2980−2987.
(21) Schultz, P. *SeqQuest Code Project*; Sandia National Laboratories (http://www.cs.sandia.gov/~paschul/Quest/).
(22) Loukrakpam, R.; Luo, J.; He, T.; Chen, Y.; Xu, Z.; Njoki, P. N.; Wanjala, B. N.; Fang, B.; Mott, D.; Yin, J.; et al. *J. Phys. Chem. C* **2011**, *115*, 1682−1694.
(23) Sha, Y.; Yu, T. H.; Liu, Y.; Merinov, B. V.; Goddard, W. A. *J. Phys. Chem. Lett.* **2010**, *1*, 856−861.
(24) Mills, G.; Jonsson, H.; Schenter, G. K. *Surf. Sci.* **1995**, *324*, 305−337.
(25) Mills, G.; Jonsson, H. *Phys. Rev. Lett.* **1994**, *72*, 1124−1127.
(26) Jacob, T.; Goddard, W. A. *ChemPhysChem* **2006**, *7*, 992−1005.
(27) Sha, Y.; Yu, T. H.; Merinov, B. V.; Shirvanian, P.; Goddard, W. A. *J. Phys. Chem. Lett.* **2011**, *2*, 572−576.
(28) Clay, C.; Haq, S.; Hodgson, A. *Phys. Rev. Lett.* **2004**, *92*, 046102.
(29) Marković, N. M.; Ross, P. N., Jr. *Surf. Sci. Rep.* **2002**, *45*, 117−229.
(30) Bondarenko, A. S.; Stephens, I. E. L.; Hansen, H. A.; Pérez-Alonso, F. J.; Tripkovic, V.; Johansson, T. P.; Rossmeisl, J.; Nørskov, J. K.; Chorkendorff, I. *Langmuir* **2011**, *27*, 2058−2066.
(31) Hammer, B.; Norskov, J. K. *Surf. Sci.* **1995**, *343*, 211−220.
(32) Hammer, B.; Norskov, J. K. *Nature* **1995**, *376*, 238−240.
(33) Stephens, I. E. L.; Bondarenko, A. S.; Gronbjerg, U.; Rossmeisl, J.; Chorkendorff, I. *Energy Environ. Sci.* **2012**, *5*, 6744−6762.
(34) Sha, Y.; Yu, T. H.; Merinov, B. V.; Goddard, W. A. *J. Phys. Chem. C* **2012**, *116*, 6166−6173.
(35) Rossmeisl, J.; Karlberg, G. S.; Jaramillo, T.; Norskov, J. K. *Faraday Discuss.* **2009**, *140*, 337−346.